

Supporting Information

Enhanced Photoresponse of Indium-Doped Tin Disulfide Nanosheets

*Shuo Yuan¹, Chao Fan^{1, *}, He Tian¹, Yonghui Zhang¹, Zihui Zhang¹, Mianzeng*

*Zhong³, Hongfei Liu⁴, Mengjun Wang¹ and Erping Li^{1, 2, *}*

¹Institute of Micro-Nano Photoelectron and Electromagnetic Technology Innovation, School of Electronics and Information Engineering, Hebei University of Technology, Tianjin, 300401, China.

²Key Laboratory of Advanced Micro/Nano Electronic Devices & Smart Systems of Zhejiang, Zhejiang University, Hangzhou 310027, China.

³Institute of Super-microstructure and Ultrafast Process in Advanced Materials, School of Physics and Electronics, Central South University, Changsha 410083, China.

⁴School of Science, Tianjin Chengjian University, Tianjin 300384, China.

Corresponding Authors

* fanch@hebut.edu.cn (C. Fan)

* liep@zju.edu.cn (E. Li).

Contents list

Fig. S1 Thickness of the pristine N-SnS₂.

Fig. S2 Structural models of DFT calculations.

Fig. S3 Formation process of In-doped N-SnS₂.

Fig. S4 Optoelectronic characterization of the photodetectors based on the pristine and In-doped N-SnS₂.

Fig. S5 Comparison and analyzation of the performances of the photodetectors based on the pristine and In-doped N-SnS₂.

Fig. S6 UV reflectance spectra and $(F(R)h\nu)^{1/2}-h\nu$ curves of the pristine and In-doped N-SnS₂.

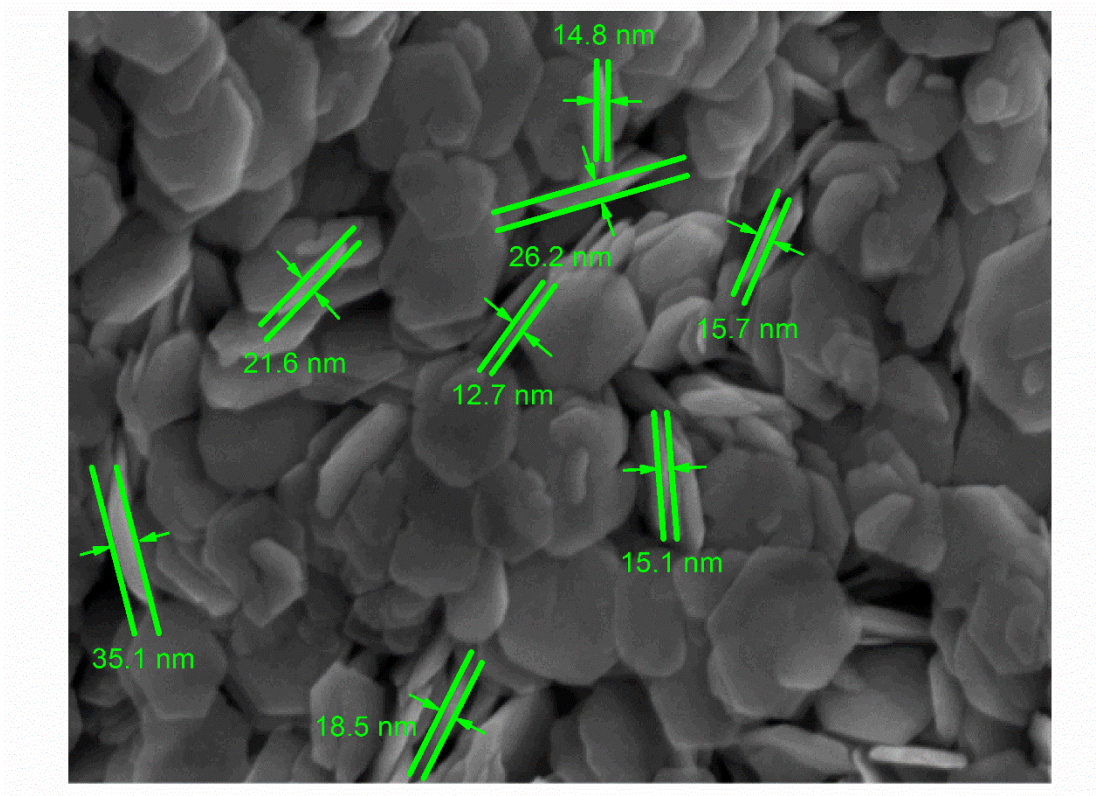


Figure S1 Thickness of the pristine N-SnS₂.

As shown in Fig. S1, the pristine N-SnS₂ have an average thickness of ~20 nm.

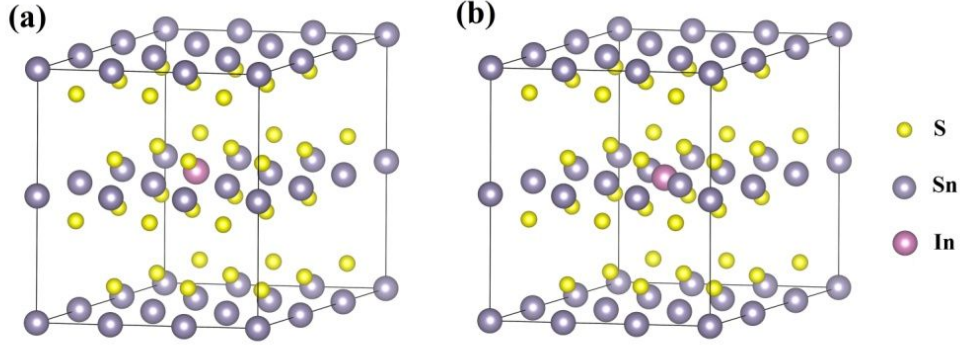


Figure S2 Structural models of DFT calculations. (a) In substitution for Sn. (b) In intralayer intercalation.

First-principles calculations are performed using the Vienna ab initio simulation package on the basis of density-functional theory^{1,2}. The exchange-correction interaction is treated by the generalized gradient approximation (GGA) with Perdew-Burke-Ernzerhof (PBE) functional³. The valence electron configurations considered in this work are In ($4d^{10}5s^25p^1$), Sn ($4d^{10}5s^25p^2$) and S ($3s^23p^4$), respectively. We simulate the In-doped SnS_2 system by using the $3 \times 3 \times 2$ repetition of a unit bulk SnS_2 cell (54-atom). The configurations of In substitution and intralayer intercalation in the SnS_2 supercell are shown in Figure 1. The cutoff energy is set to be 500 eV and the convergence accuracy of the self-consistent calculation is 10^{-5} eV. The Monkhorst-Pack grids of $3 \times 3 \times 3$ are used for Brillouin zone integrations⁴. All atoms in SnS_2 and In-doped SnS_2 are fully relaxed until the components of residual forces are smaller than 0.05 eV/Å.

We have calculated the formation energy (E_f) by assuming the Sn and In atom reservoirs are bulk Sn and bulk In, thus $E_f = E_{\text{doped}} - E_0 - nE_{\text{In}} + mE_{\text{Sn}}$ ⁵, where E_{doped} , E_0 , E_{In} and E_{Sn} are the total energy of In-doped SnS_2 , pure SnS_2 , bcc In and fcc Sn, respectively. The integers n and m are the number of doped In atoms and substituted Sn atoms, respectively. The calculated formation energies of substitutional and intralayer intercalated Indium defects are 0.85 and 4.63 eV, respectively. Thus, the substitution of In can be easily generated than intralayer intercalation of In in SnS_2 .

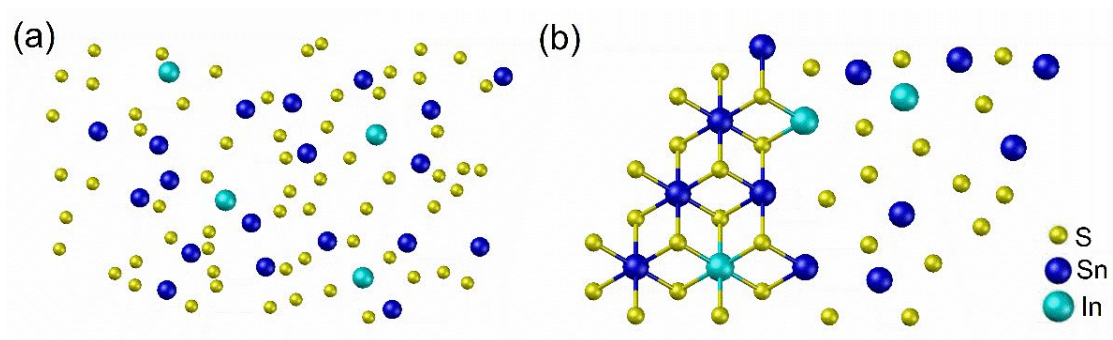


Figure S3 Formation process of In-doped N-SnS₂. (a) Ions were dispersed in the solution (b) Formation of SnS₂ and In substitutions.

During the hydrothermal process, In, Sn, and S ions were dispersed and distributed uniformly in the aqueous solution, as shown in Fig. S3 (a). In certain reaction conditions, Sn and S ions interacted and bonded. Meanwhile, In ions also interacted with S ions and substituted for Sn as shown in Fig. S3 (b).

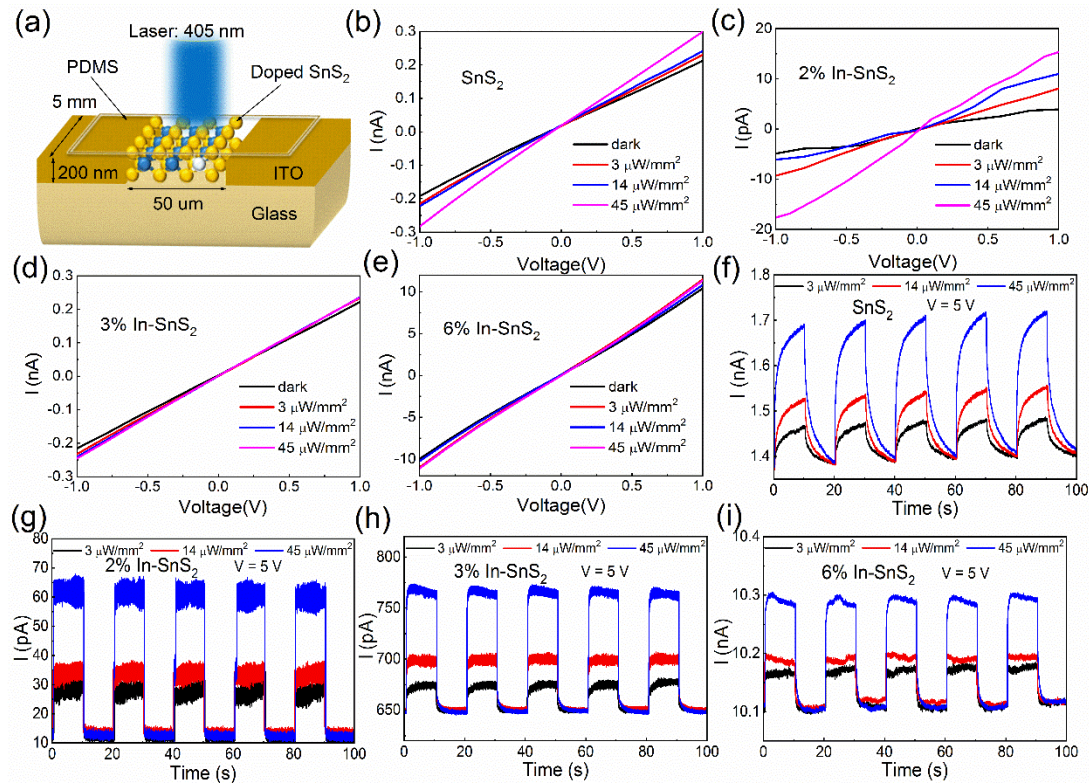


Figure S4 Optoelectronic characterization of the photodetectors based on the pristine and In-doped N-SnS₂. (a) Schematic diagram of a typical In-doped N-SnS₂ photodetector; The current-voltage (*I-V*) characteristics of the devices based on the (b) N-SnS₂, (c) 2 at%, (d) 3 at%, and (e) 6 at% In-doped N-SnS₂ under illumination with a blue 405-nm laser of different power intensities; The current-time (*I-T*) characteristics of the devices based on the (f) N-SnS₂, (g) 2 at%, (h) 3 at% and (i) 6 at% In-doped N-SnS₂.

Similar to the performances under illumination with a green 532-nm laser, *I-V* curves under illumination with a blue 405-nm laser show the contacts between the as-prepared pristine and In-doped N-SnS₂ were Ohmic contacts. *I-T* curves in Fig. S2 (f)-(i) show *I* varied up and down repeatedly, which demonstrate the devices were stable and repeatable. They all show a multiple growth as power intensity increased exponentially.

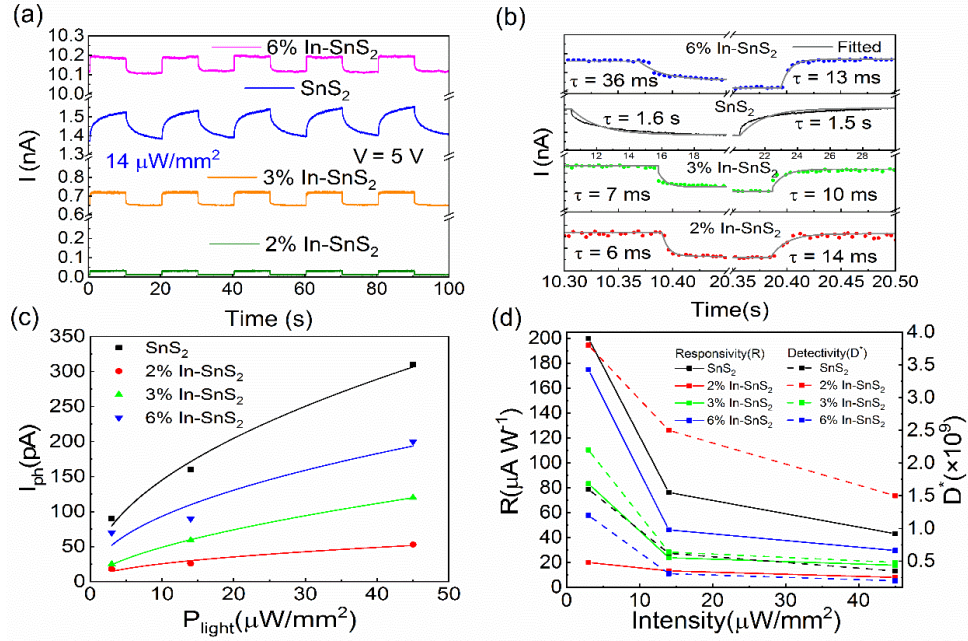


Figure S5 Comparison and analysis of the performances of the photodetectors based on the pristine and In-doped N-SnS₂. (a) Time-resolved photoresponse of photodetectors based on the pristine and In-doped N-SnS₂; (b) Single high-resolution photoresponse of photodetectors; (c) Dependence of photocurrent on the incident power intensity; (d) Responsivity and detectivity of photodetectors.

Fig. S3(a) shows I - T curves of the photodetectors under illumination with a blue laser of the same power intensity of 14 $\mu\text{W}/\text{mm}^2$. Dark current of the photodetectors based on the In-doped N-SnS₂ were lower than that for the pristine N-SnS₂ photodetector, except for the 6 at% In-doped N-SnS₂ photodetector. The photoresponse time including the rise and fall time for the In-doped N-SnS₂ were much less than that for the pristine N-SnS₂. The photodetector of the 3 at% In-doped N-SnS₂ showed fastest photoresponse to 50 mHz illumination. Fig. S3(c) depicts the scatter plots of I_{ph} - P which are fit by the equation of $I_{ph} = aP_{light}^\alpha$. The fit parameter α are 0.50 for the pristine N-SnS₂, 0.47 for the 2 at% In-doped N-SnS₂, 0.59 for the 3 at% In-doped N-SnS₂ and 0.48 for the 6 at% In-doped N-SnS₂. At the power intensity of 14 $\mu\text{W}/\text{cm}^2$, the responsivity (R) and detectivity (D^*) are 76.2 $\mu\text{A} \cdot \text{W}^{-1}$ and 6.2×10^8 for the pristine SnS₂, 13.3 $\mu\text{A} \cdot \text{W}^{-1}$ and 2.5×10^9 for the 2 at% In-doped N-SnS₂, 23.8 $\mu\text{A} \cdot \text{W}^{-1}$ and 6.4×10^8 for the 3 at% In-doped N-SnS₂, 46.2 $\mu\text{A} \cdot \text{W}^{-1}$ and 3.1×10^8 for the 6 at% In-doped N-SnS₂.

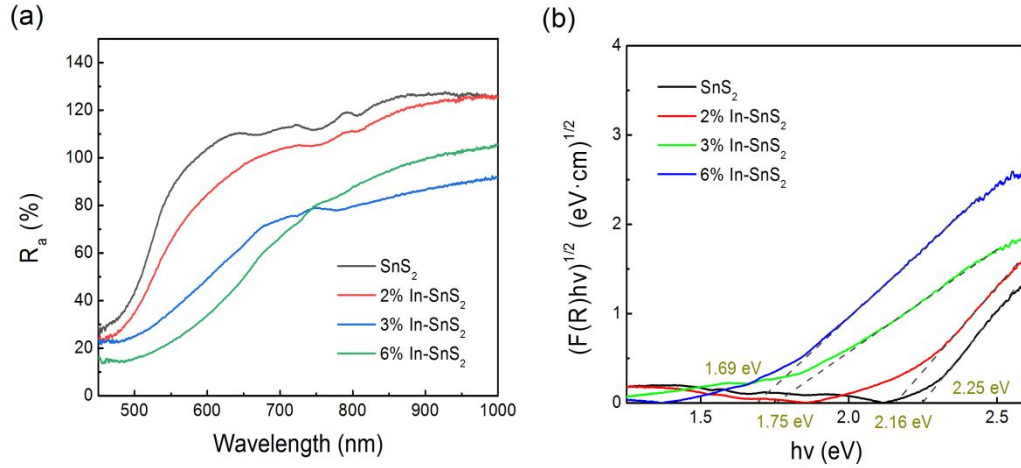


Figure S6 (a) UV reflectance spectra and (b) $(F(R)hv)^{1/2}$ - hv curves of the pristine and In-doped N-SnS₂.

The UV reflectance spectra of the as-prepared samples from 400 to 1000 nm are shown in Fig. S4(a). The results indicate that In doping enhanced the optical absorption capability of the N-SnS₂. Moreover, the optical band gap energies were estimated from the UV–visible diffuse reflection spectra by using the Kubelka-Munk relation to convert the reflectance into a Kubelka-Munk function (equivalent to the absorption coefficient). The Kubelka-Munk relation is expressed as the following equation: $F(R_a) = (1-R_a)^2/2R_a$, where R_a is the reflectance of the as-prepared samples with respect to a reference at each wavelength. The curves of $(F(R)hv)^{1/2}$ - hv for the pristine and In-doped N-SnS₂ are plotted in Fig. S4(b), hv is the discrete photon energy. Bandgap energies are 2.25 eV for the pristine SnS_2 , 2.16 eV for the 2 at% N-SnS₂, 1.75 eV for the 3 at% N-SnS₂ and 1.69 eV for the 6 at% N-SnS₂, respectively.

REFERENCES

- [1] Kresse, G.; Hafner, J. Ab Initio Molecular Dynamics for Liquid Metals Phys. Rev. B 1993, 47, 558–561.
- [2] Kresse, G.; Furthmüller, J. Efficient Iterative Schemes for Ab Initio Total-Energy Calculations Using a Plane-Wave Basis Set Phys. Rev. B 1996, 54, 11169–11186.
- [3] Perdew, J. P.; Burke, K.; Ernzerhof, M. Generalized Gradient Approximation Made Simple Phys. Rev. Lett. 1996, 77, 3865–3868.
- [4] Monkhorst, H. J.; Pack, J. D. Special Points for Brillouin-Zone Integrations Phys. Rev. B 1976, 13, 5188–5192.
- [5] Cui, X. Y.; Medvedeva, J. E.; Delley, B.; Freeman, A. J.; Newman, N.; Stampfl, C. Role of Embedded Clustering in Dilute Magnetic Semiconductors: Cr Doped GaN Phys. Rev. Lett. 2005, 95, 256404.